Spatial behavior of energy relaxation of electrons in capacitively coupled discharges: Comparison between Ar and SiH_4

M. Yan,[a] A. Bogaerts, and R. Gijbels
Department of Chemistry, University of Antwerp (UIA), Universiteitsplein 1, B-2610 Wilrijk-Antwerp, Belgium

W. J. Goedheer
FOM-Institute for Plasma Physics ''Rijnhuizen,'' P.O. Box 1207, 3430 BE Nieuwegein, The Netherlands

(Received 22 September 1999; accepted for publication 12 January 2000)

The electron energy relaxation in space has been investigated for electropositive Ar and electronegative SiH_4 discharges by a 1D Particle-in-cell/Monte Carlo code. The ionization rate has been studied since this rate is strongly influenced by the energy relaxation mechanism. The ionization rate in the two kinds of discharges at a low pressure (30 mTorr), a low power (8 W), and a low frequency (13.56 MHz) is regarded as the reference case. The effects of pressure, power, and frequency on the ionization rate have been observed and compared between the two types of discharges. With the pressure increasing from 30 to 400 mTorr, in the case of the argon discharge the ionization peak moves from the plasma bulk (nonlocal behavior of the electron energy distribution function) towards the momentary cathodic presheath (local behavior). In addition to a similar variation of the ionization rate, in the silane discharge an ionization peak occurs near the momentary anodic presheath, and at the high pressure the ionization in the plasma bulk is still considerable. The power can only influence the ionization rate quantitatively. The effect of frequency on the ionization rate is similar for both kinds of discharges. With increasing frequency the ionization rate tends to a somewhat local character, i.e., the ionization appears closer to the momentary cathode. This is attributed to the fact that at the high frequency a bulk electric field in the bulk is found clearly out of phase with the sheath fields, and the energetic electrons are pushed towards the cathode earlier in space. Meanwhile, in the silane discharge the distinctive ionization, which is strongly present at the anodic presheath and in the plasma bulk at low frequency, almost disappears. © *2000 American Institute of Physics.* [S0021-8979(00)02608-6]

I. INTRODUCTION

Plasma processing based on rf glow discharges is widely used in the microelectronics industry.[1,2] Understanding the basic principles governing the behavior of glow discharges is mandatory in optimizing plasma processing.

For the behavior of the electrons in a rf discharge, energy relaxation lengths are important because they contain the information of the energy gain process from the oscillating electric field and energy loss process due to inelastic collisions. Spatial energy relaxation depends on the ratio between the mean free path for energy loss and the relevant length scales in the discharges. The pressure can influence the spatial relaxation process dramatically. In low-pressure gas discharges, inelastic collisions occur at a rather lower frequency so that the electrons diffuse over a long distance before their energy changes (elastic collisions mainly change the momentum, not the energy), this gives rise to so-called nonlocal effects influencing the electron energy distribution function (EEDF). On the other hand, at high pressures the energy relaxation length is shorter than the characteristic spatial scale of the plasma, i.e., the energetic electrons lose their energy before they can diffuse a long distance, and a local behavior is exhibited. In the nonlocal situation, the EEDF at a certain position depends on processes taking place at other positions, while in the local situation, the EEDF is only based on the local processes.

Plasma enhanced material processing equipment (deposition or etching) is often operated at a very low pressure (i.e., from 1 to hundreds of mTorr) and at a high frequency (i.e., from 10 to 100 MHz). The electron energy relaxation in space behaves quite differently in this range of discharge settings. The ionization rate may be used to illustrate and describe the behavior of the electron energy relaxation because this rate relies closely on the behavior of the energetic electrons. In many publications the ionization rate is discussed (e.g., Refs. 3–6), but not very systematically or addressing different aspects. The effect of pressure (from 30 to 300 mTorr) on the time-averaged ionization rate in the helium discharge has been studied by Surendra,[7] and the effect of applied frequency (from 13.56 to 54.24 MHz) on the time-averaged ionization rate with a constant voltage has been observed in the argon discharge by Colgan and co-workers.[8]

In this article we focus on the study of the spatiotemporal variation of the ionization in order to understand the electron energy relaxation. The detailed modulation of ionization in space and time will be analyzed. The effects of pressure, power, and frequency on the ionization rate are studied while keeping the other parameters constant, so that the results are

[a]Electronic mail: yan@uia.ua.ac.be

easy to compare and interpret. Moreover, since the inelastic collisions occur almost over the whole energy range in molecular gas discharges such as the silane discharge, this leads to differences of the energy relaxation compared to rare gas discharges such as argon and helium discharges. Furthermore, the electropositive and electronegative discharges have quite different electric characteristics. Therefore, in this article the difference of the energy relaxation between electropositive rare gas discharges (argon) and electronegative molecular gas discharges (silane) will be investigated and clarified.

Self-consistent fluid models coupling the charged particle transport and the electric field have been widely used to study electropositive as well as electronegative rf discharges (e.g., Refs. 9–12). Such fluid models have described and explained many basic characteristics and phenomena observed in experiments. However, the collision rates calculated in fluid models are based on the local approximation, i.e., the distribution function and the electric field are assumed not to vary strongly in space and in time. Therefore, fluid models are rather restricted to high-pressure situations.

The theory for discharges in the nonlocal regime was first formulated by Bernstein and Holstein[13] and was developed later by Tsendin.[14] This nonlocal approach method has been applied in modeling of low-pressure capacitively coupled rf electropositive discharges.[15] This method is based on the fact that the EEDF can be solved in an analytical or semi-analytical way at very low pressure. However, this method is restricted by many assumptions. For example, the discharge frequency should be much higher than the inelastic collision frequency. Hence, this nonlocal approach method can hardly be applied to mixtures of molecular gas discharges such as SiH_4 discharges because the inelastic collision frequency for such discharges can be comparable to the discharge frequency over practically the whole energy range.[16]

Particle-in-cell/Monte Carlo (PIC/MC) simulations can describe both the nonlocal and the local behavior of the electron energy relaxation very accurately because they treat the charged particles in a kinetic way without making use of restrictive assumptions. This method can demonstrate the evolution of the electron energy relaxation in a relatively wide range of discharge parameters. The major disadvantage of this method is that it is very time consuming. At high electron densities, the Debye length becomes small, and hence, fine grids are needed. More particles have to be followed to keep the statistical fluctuations low enough. That requires long calculation times. Moreover, for electronegative discharges, the negative ions are confined in the plasma, and the only loss mechanism, i.e., recombination with positive ions, is very slow, which results in a very low convergence speed. Therefore, the PIC/MC method is usually applied to low-pressure electropositive discharges such as argon or helium discharges,[17–19] and only very few PIC/MC calculations are used to study electronegative discharges, e.g., oxygen discharges.[18]

For the simulation of electronegative discharges, we have developed a global particle balance method in our 1D and 2D PIC/MC models to considerably speed up the convergence toward a periodic steady state (see later and Ref. 20). Furthermore, in our study the pressure ranges from a few tens of to a few hundreds of millitorr, and the PIC/MC model still provides sufficient speed and accuracy. Since in this article we focus on the influence of pressure, power, and frequency on the ionization rate, a 1D model is sufficient to reveal the relevant physics in this study of argon and silane discharges. So all the results presented here are obtained from our 1D PIC/MC model.

In Sec. II of this article, the PIC/MC model, the collisions involved for the two kinds of discharges, and the simulation parameters will be given. In Sec. III, the calculated ionization rates for argon and silane discharges versus pressure, power, and frequency are investigated. Finally, a summary is given in Sec. IV.

II. MODEL DESCRIPTION

A. PIC/MC model

The PIC/MC method is based on a kinetic description of the particle motion in phase space. Charged ''superparticles'' move in the self-consistent electric field which they generate. A Monte Carlo formalism is used to describe the effect of collisions. The PIC/MC method has been described in detail by Birdsall[17] and Vahedi and Surendra.[18] We have developed our own PIC/MC codes and we have improved the calculation speed for the electronegative SiH_4 discharge by using the global particle balance method.[20] The general idea of this method is based on the condition that in the quasisteady state, a balance should be achieved on average between the production and loss of each type of particles. The balance with the longest time scale, the negative ion balance (attachment and recombination), is chosen as a criterion in this particle balance method. After some cycles, an increment α_0 for guessing the new ion densities $[\rho_i' = \rho_i(1+\alpha_0)]$ is calculated as $\alpha_0 = (1+\Delta)^{1/2} - 1$, where $\Delta = (R_{\mathrm{att}} - R_{\mathrm{rcm}})/R_{\mathrm{rcm}}$ is the relative difference between the attachment rate R_{att} and recombination rate R_{rcm}, and ρ_i and ρ_i' are the old and the new ion density, respectively; R_{att} and R_{rcm} can be obtained from the previous cycles of the simulation. In the calculations the new ion density is obtained by changing the superparticle's size. Consequently, the net charge in the discharge changes and has to be balanced by an opposite charge on the wall. This amount of net charge is distributed over the two electrodes according to the charge distribution obtained before the adjustment of the ion density. Meanwhile, the velocity and the energy of the particles are kept the same. This procedure reduces the calculation time that the code would run from a lower density to this new density, and the calculation restarts immediately at a density closer to the one in the final quasisteady state. A picture comparing the two simulations, either with and without the particle balance has been presented in Ref. 20. The scheme representing this particle balance method is shown in Fig. 1.

B. Particle collisions

For the argon discharge, there are two kinds of charged particles in our 1D PIC/MC model: electrons e^- and ions

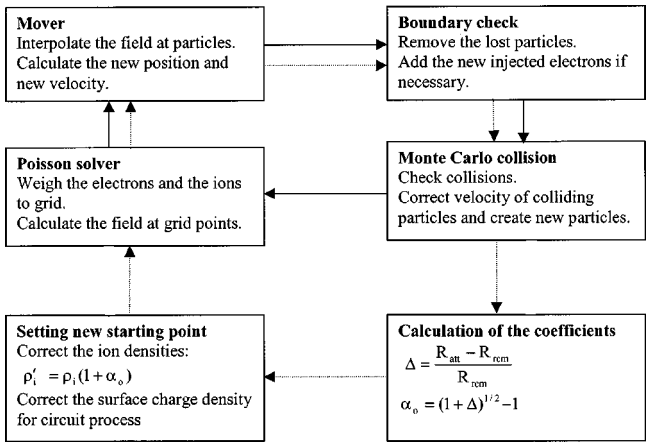

FIG. 1. The scheme of the PIC/MC simulation process with the particle balance method. The dashed arrow routine is switched on for one time step after running many cycles in the solid arrow routine.

Ar^+. The electron and ion impact collisions included in the model are shown in Table I. The cross sections are taken from the references given in the table.

For the silane discharge, we simplify the situation by considering a pure silane gas. The charged particles in our model are electrons (e^-), positive ions (SiH_3^+) and negative ions (SiH_3^-). The assumption taking into account only the SiH_3^+ as positive ions is justified by Hamer's measurement.[21] In Table II we give the reactions caused by electron and ion impact which are included in the code for the SiH_4 discharge. The cross sections are again taken from the references in the table. Ion-neutral elastic collision cross sections are obtained according to the Langevin formula.[30] The collisions are supplemented with the null collision in order to have a collision frequency independent of energy[18] except the recombination. The number of positive ion and negative ion recombination events during a certain time interval is obtained from the integral of the product of the recombination rate coefficient k_{rcm} and the ion densities over the whole discharge range. The recombination event is treated for the negative ion. The positive ions are considered as the targets, and the recombination takes place with the nearest positive ion.

Reactions between radicals are not included in our codes because we do not focus on chemistry, but on the electron energy relaxation due to electron impact inelastic collisions.

TABLE I. Collisions included in the model for the argon discharge.

Type	Reaction	Threshold energy (eV)	Ref.
Elastic collision	$e+Ar \rightarrow e+Ar$		22
Excitation	$e+Ar \rightarrow e+Ar^*$	12.0	22
Ionization	$e+Ar \rightarrow 2e+Ar^+$	15.7	22
Elastic collision	$Ar^+ + Ar \rightarrow Ar^+ + Ar$		18
Charge transfer	$Ar^+ + Ar \rightarrow Ar + Ar^+$		18

TABLE II. Collisions included in the model for the silane discharge.

Type	Reaction	Threshold energy (eV)	Ref.
Elastic collision	$SiH_4+e^- \rightarrow SiH_4+e^-$		23
Vibrational excitation	$SiH_4+e^- \rightarrow SiH_4^a+e^-$	0.27	24
Vibrational excitation	$SiH_4+e^- \rightarrow SiH_4^b+e^-$	0.11	24
Ionization	$SiH_4+e^- \rightarrow SiH_3^+ + 2e^- + H$	13.0	25
Attachment	$SiH_4+e^- \rightarrow SiH_3^- + H$	5.7	26
Dissociation	$SiH_4+e^- \rightarrow SiH_n + e^- + (4-n)H$	8.3	27
H^- transfer	$SiH_3^+ + SiH_4 \rightarrow SiH_4^* + SiH_3^+$		28
Recombination	$SiH_3^+ + SiH_3^- \rightarrow SiH_3 + SiH_3$		29
Elastic collisions	$SiH_3^+ + SiH_4 \rightarrow SiH_3^+ + SiH_4$		30

[a]Vibrational excitation 2–4.
[b]Vibrational excitation 1–3.

C. Simulation parameters

In the following simulations, only the 1D situation is considered. The distance between the two electrodes is 3 cm. The electrode area is 200 cm^2. The background gas (feed gas) is regarded as uniform and the gas pressure is fixed during the simulation. To make further simplification, the secondary electron emission coefficient and reflection coefficient from the electrodes are assumed to be zero.

The ionization rate is calculated as a function of pressure, power, and frequency. During the study of the influence of one specific parameter on the ionization rate, the other parameters are kept constant. The discharge with a pressure of 30 mTorr, a power of 8 W, and a frequency of 13.56 MHz is considered as a reference for the following simulations and comparisons. The parameter settings for the three other situations are 400 mTorr, 8 W, and 13.56 MHz for studying the pressure effect, 30 mTorr, 25 W, and 13.56 MHz for studying the power effect, and 30 mTorr, 8 W, and 65 MHz for studying the frequency effect, respectively.

In the present simulation, we chose 64 and 100 spatial grid points for different density cases, and 1000 time steps in one rf cycle. Several thousands of superparticles for each type of charged particle are followed. In the simulations of the argon discharge, the superparticle size for the electrons and the argon ions is the same. For the silane discharge, the superparticle size for the electrons is chosen one order of magnitude lower than for the ions due to the much lower electron density compared to the ions.

III. RESULTS AND DISCUSSION

A. The argon discharge

1. Pressure effect

Figure 2 shows the spatiotemporal electric field (a) and electron density profile (b) during one rf cycle for the argon discharge at a frequency of 13.56 MHz, a power of 8 W, and a pressure of 30 mTorr. Similar pictures can be found in other papers, e.g., Refs. 10 and 11. We show these pictures here again in order to explain more easily the behavior of the ionization rate. The axis at $z=0$ is the rf powered electrode,

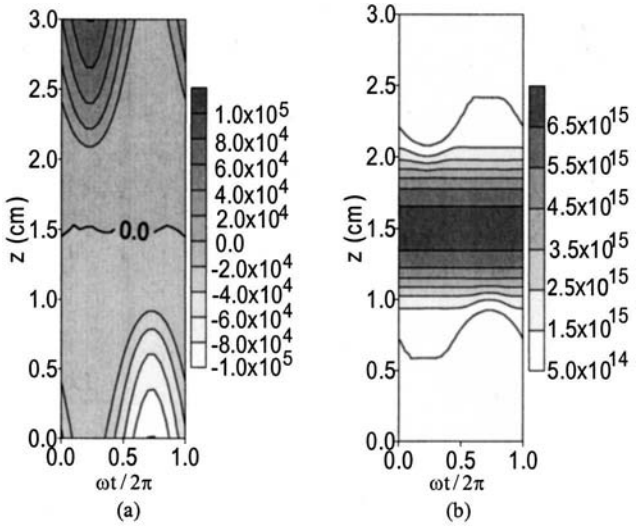

FIG. 2. The variations of (a) electric field (V/m) and (b) electron density (m^{-3}) in space and time (one cycle) for the argon discharge. The discharge settings are a pressure at 30 mTorr, a power at 8 W, and a frequency at 13.56 MHz.

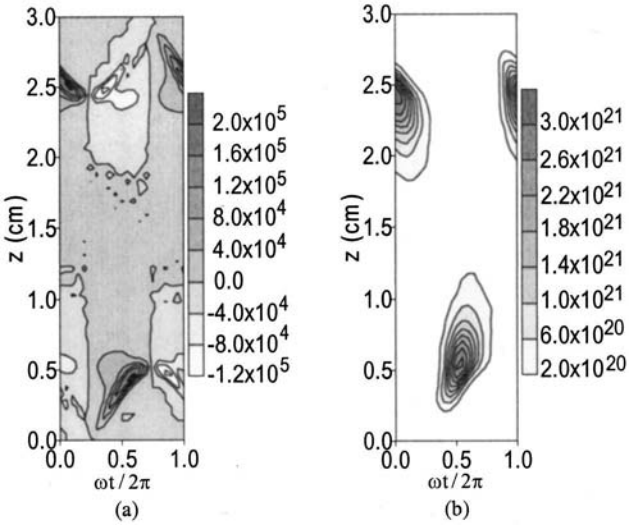

FIG. 4. The variations of (a) electron heating ($W\,m^{-3}$) and (b) ionization rate ($m^{-3}\,s^{-1}$) in space and time for the argon discharge at a higher pressure of 400 mTorr. The other parameters are the same as in Fig. 2.

and the one at $z=3$ cm is the grounded electrode. The phase axis ($\omega t/2\pi$) shows the variation of one rf cycle. As shown in Fig. 2(a), the electric field varies in time mainly in the sheaths during one rf cycle, while the field reversal point remains in the plasma bulk center [marked by a thicker curve in Fig. 2(a)] and does not change much versus time. The latter phenomenon is important for further explanations (see later). The electron density profile is shown in Fig. 2(b). The electrons are pushed away from the momentary cathode by the strong electric field there and move towards the momentary anode due to the sheath contraction. The maximum electron density is in the plasma bulk and remains constant during the entire cycle.

The ionization rate is studied here versus feed gas pressure for the argon discharge. Figures 3(a) and 3(b) show the spatial and temporal electron heating ($-e\Gamma_e E$) and ionization rate at 30 mTorr. The difference in positions of the electron energy gain due to the heating and loss due to the inelastic collisions is compared. In Fig. 3(a), one peak of electron heating [the dark part in Fig. 3(a)] covers in space the range from the cathode towards the maximum sheath width during the sheath expanding part, and one peak of electron energy loss [the light part in Fig. 3(a)] covers the range from the maximum sheath width towards the anode during the sheath contracting, halfway through the rf cycle. The zero contour line is shown as a thicker line to distinguish between energy gain and energy loss in all of the following electron heating profiles. Similarly, one ionization peak appears at the same phase as the electron heating peak but it is located almost in the plasma bulk as is shown in Fig. 3(b). This phenomenon is a typical feature of a nonlocal behavior of the energy relaxation in space, i.e., the electron energy relaxation length is longer than the plasma characteristic scale. In other words, the electrons can bring the energy gained during the sheath expansion at the presheath to the plasma bulk and produce ionization there. A similar picture has been shown in other PIC simulations of rf helium and hydrogen discharges.[31,32]

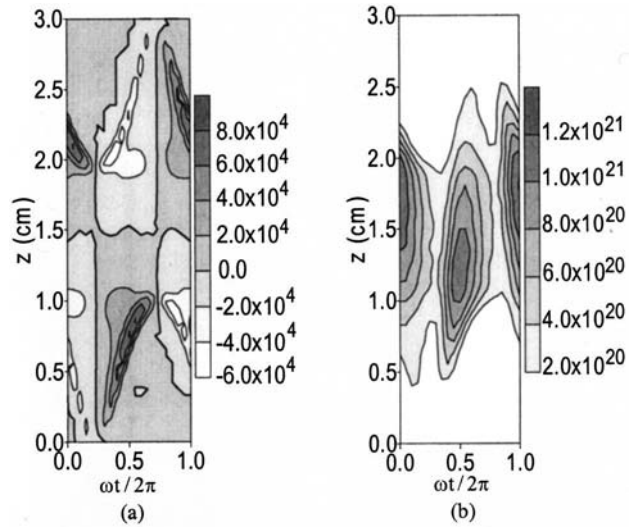

FIG. 3. The variations of (a) electron heating ($W\,m^{-3}$) and (b) ionization rate ($m^{-3}\,s^{-1}$) in space and time of the argon discharge with the same discharge settings as in Fig. 2.

Figures 4(a) and 4(b) show the evolution of the same variables as in Fig. 3 but now at a pressure of 400 mTorr. The electron heating behaves similarly to the low pressure. However, the peak is narrower in space and closer to the electrode due to the thinner sheath at the high pressure, and the absolute value of the electron heating increases. The ionization peak on the other hand, shows a quite different spatial behavior compared to the low-pressure case shown in Fig. 3(b). The peak occurs at a position much closer to the heating peak and there is almost no ionization in the plasma bulk. This is typical for the local behavior of the energy relaxation in space, where the energy relaxation length at high pressure is so short that the electrons gain energy near the presheath

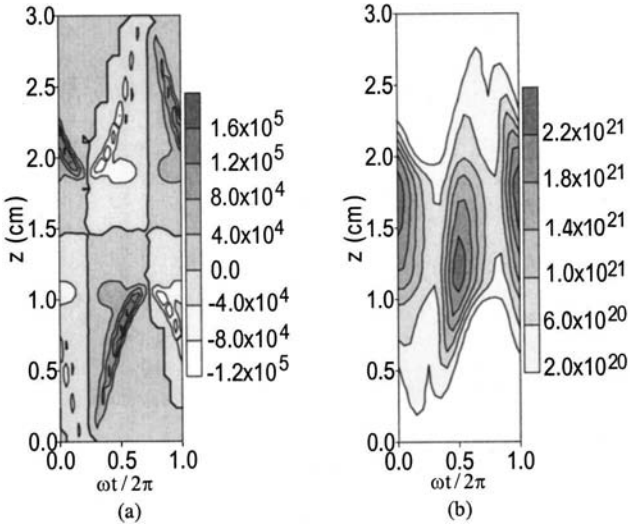

FIG. 5. The variations of (a) electron heating ($W\,m^{-3}$) and (b) ionization rate ($m^{-3}\,s^{-1}$) in space and time for the argon discharge at a higher power of 25 W. The other parameters are the same as in Fig. 2.

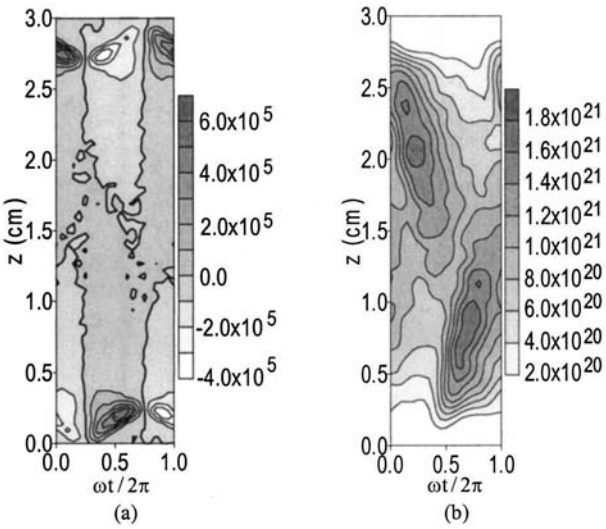

FIG. 6. The variations of (a) electron heating ($W\,m^{-3}$) and (b) ionization rate ($m^{-3}\,s^{-1}$) in space and time for the argon discharge at a high frequency of 65 MHz. The other parameters are the same as in Fig. 2.

but cannot move a long distance before the energies are relaxed through the inelastic collisions.

In addition, we found that the bulk electric field at high pressure (not shown) is different from the lower pressure case [in Fig. 2(a)]. Indeed, at low pressure the bulk field does not vary with time. At high pressure, however, we found that a weak bulk field is clearly out of phase with the sheath fields. A similar behavior has been found by the measurement of Sato and Lieberman in an argon rf discharge[33] and by the simulation of Sommerer and co-workers for a helium rf glow discharge.[34]

2. Power effect

The effect of power on the ionization rate has been studied with the frequency fixed at 13.56 MHz and the pressure fixed at 30 mTorr. The spatiotemporal electron heating and ionization rate are shown in Figs. 5(a) and 5(b) for a higher power value of 25 instead of 8 W in Fig. 3. It is clear that the spatiotemporal behavior of electron heating and ionization rate is more or less the same as the low power case in Fig. 3 except that the absolute values are higher due to the higher power input.

3. Frequency effect

The effect of frequency on the ionization rate has been studied with a fixed pressure of 30 mTorr and a fixed power of 8 W. The spatiotemporal dependence of electron heating and ionization rate are shown in Figs. 6(a) and 6(b), respectively, for a frequency of 65 compared to 13.56 MHz in Fig. 3. The behavior at high frequency seems to be quite different from that at lower frequency. The sheath expansion and contraction is much less pronounced than at low frequency, which can be deduced from the position of the electron heating peaks in Fig. 6(a). This is in part due to the lower voltage applied in order to keep the same power at high frequency. The electron heating is quite efficient and the peak value is almost one order of magnitude higher than the low frequency case. The difference of the electron heating in the plasma bulk between the low and high frequency case is considerable, which can be seen in Figs. 3(a) and 6(a). This discrepancy can be explained by the difference of the bulk electric field [see Figs. 2(a) and 7 later]. Indeed, we find that at high frequency there is a weak bulk electric field, which is strongly out of phase with the sheath fields as shown in Fig. 7. This behavior of the plasma bulk field with increasing frequency is similar to what has been found with increasing pressure.[33,34]

The ionization profile in Fig. 6(b) shows that the energetic electrons still can penetrate into the plasma bulk to some extent leading to a large amount of ionization. However, the ionization peak occurs somewhat delayed in comparison to the heating peak, and moreover it is only considerable in half of the plasma bulk while at the low frequency

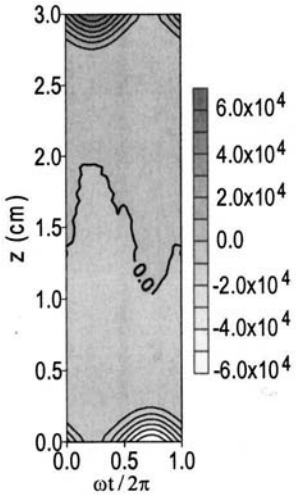

FIG. 7. The variation of electric field (V/m) in space and time at the high frequency for the argon discharge. The discharge settings are the same as in Fig. 6.

case it occurs in almost the whole plasma bulk [Fig. 3(b)]. The delay in phase can be explained by the fact that at the higher frequency (65 MHz) the electrons cannot follow the time-varying electric field. The shorter penetration into only half of the plasma bulk was also found in the simulated time-averaged ionization profile and the measured time-averaged emission intensity at a higher frequency (54.25 MHz) by Colgan and co-workers.[8] In that work the power at the high frequency was even higher than at low frequency due to the fixed voltage of 25 V, and one would expect that more high energy electrons were produced and, hence, that there would be more ionization in the plasma bulk. However, it was shown that two peaks [Figs. 7 and 9(d) in Ref. 8] appeared closer to the two presheaths compared to the one peak occurring in the middle of the plasma at lower frequency (13.56 MHz).

In our opinion, the shorter penetration of the energetic electrons can be explained by the fact that the bulk field is strongly out of phase with the sheath fields as shown in Fig. 7, i.e., the field reversal point occurs closer to the cathode when the sheath is around its maximum thickness. Furthermore, since the ionization is delayed with respect to the instantaneous field, the energetic electrons see this reversed field earlier in space when they leave the cathode. In other words, the accelerated length of the electrons in the plasma bulk by the field is shorter than half of the length of the plasma bulk, while this length of acceleration at the low frequency case [Fig. 2(a)] is exactly the half of the plasma bulk length. That means that the electric field in the plasma bulk starts to retard the electrons earlier in space and, hence, limits their penetration in the plasma bulk. Therefore, the spatial energy relaxation length becomes shorter at the high frequency.

B. The Silane discharge

1. Pressure effect

Figure 8 shows the spatiotemporal electric field (a) and electron density profile (b) during one rf cycle for the silane discharge at a frequency of 13.56 MHz, a power of 8 W, and a pressure of 30 mTorr. Compared to the electropositive argon discharge in Fig. 2(a), the electric field is quite different. In the whole plasma bulk the amplitude of the electric field is still rather high, a phenomenon which can be found in many studies, e.g., Refs. 5, 6, and 11. This plasma bulk field has the same phase as the sheath field, i.e., during the sheath expansion the electric field in the whole plasma bulk keeps the same direction as the sheath field and only changes sign at the momentary anodic presheath, except in a small region with field reversal halfway through the rf cycle [from 0.25 to 0.5 in phase and from 0.5 to 0.75 cm in space in Fig. 8(a)]. The zero contour line is marked by a thicker solid line in fig. 8(a), the contour with the value of 1250 V/m marked by a dashed line, and the one of -1250 V/m marked by a dash-dotted line. There is a relative maximum of the electric field at the momentary anodic presheath halfway through the rf cycle, marked by the dashed line (and dash-dotted line) in Fig. 8(a). This maximum has been found by Boeuf in the simulation of a model electronegative gas[10] and by Gottscho *et al.*,[35,36] in the experiments of BCl_3 rf discharges. Compared to the argon discharge, the electron density [in Fig. 8(b)] is very flat in the plasma bulk, but with a relative maximum corresponding to the relative maximum of the field and the small field reversal region [in Fig. 8(a)]. The flat shape is due to the recombination between positive ions and negative ions occurring at the plasma center.[6] The relative maximum is due to the opposite directions of the electric field in the plasma bulk and in the anode presheath so that the electrons are ''pushed'' to this position from the two directions.[12]

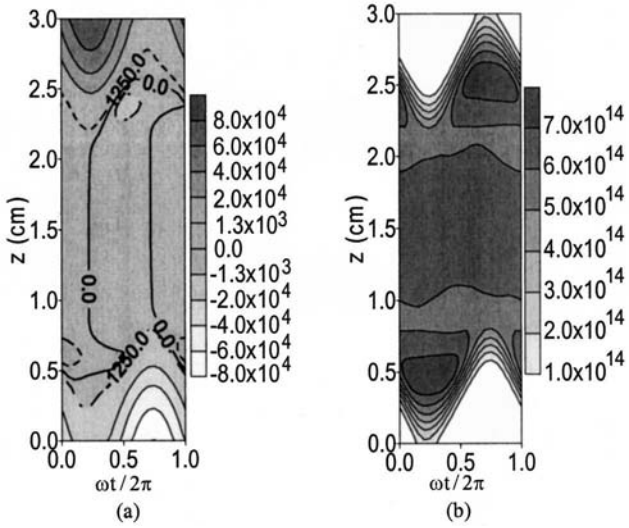

FIG. 8. The variations of (a) electric field (V/m) and (b) electron density (m^{-3}) in space and time (one cycle) for the silane discharge. The discharge settings are a pressure at 30 mTorr, a power at 8 W, and a frequency at 13.56 MHz.

Figures 9(a) and 9(b) show the spatial and temporal variations of the electron heating and ionization rate at 30 mTorr for the same discharge parameters as in Fig. 8. Compared to the argon discharge [Figs. 3(a) and 3(b)], the behavior of the electron heating and the ionization rate is similar in

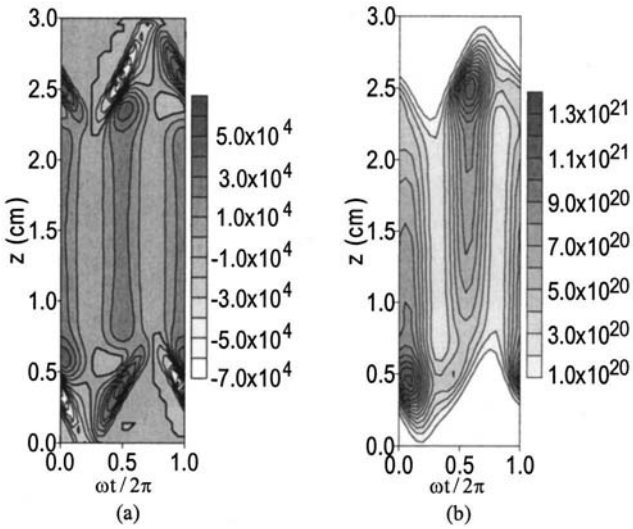

FIG. 9. The variations of (a) electron heating ($W\,m^{-3}$) and (b) ionization rate ($m^{-3}\,s^{-1}$) in space and time for the silane discharge with the same discharge settings as in Fig. 8.

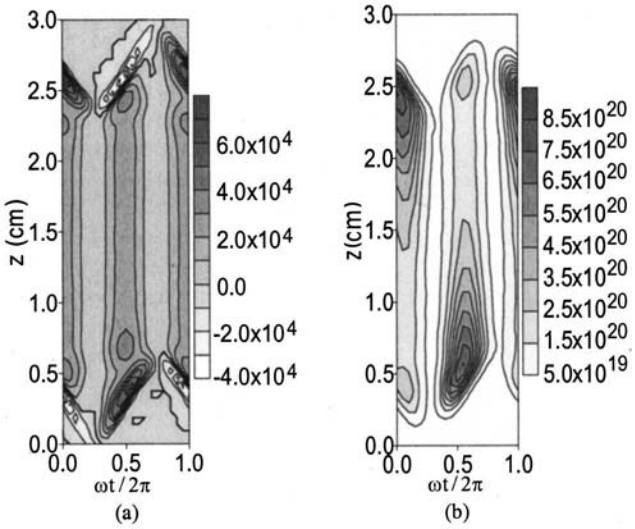

FIG. 10. The variations of (a) electron heating ($W\,m^{-3}$) and (b) ionization rate ($m^{-3}\,s^{-1}$) in space and time for the silane discharge at a higher pressure of 400 mTorr. The other parameters are the same as in Fig. 8.

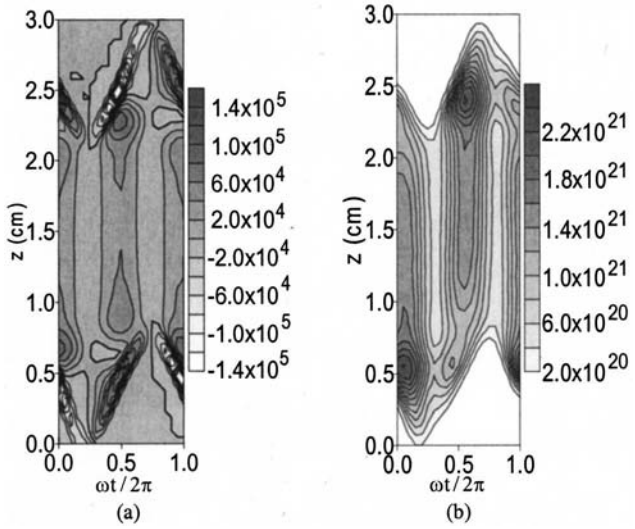

FIG. 11. The variations of (a) electron heating ($W\,m^{-3}$) and (b) ionization rate ($m^{-3}\,s^{-1}$) in space and time for the silane discharge at a higher power of 25 W. The other parameters are the same as in Fig. 8.

the sense that a pronounced electron heating peak and an electron energy loss peak appear at the momentary cathode presheath and at the anode presheath halfway through the rf cycle, and that the ionization occurs strongly in the plasma bulk. This means that the spatial energy relaxation length is very long. In addition, the electron heating in the plasma bulk is remarkable, and there is another smaller electron heating peak at the momentary anode presheath close to the energy loss peak. Moreover, the maximum of the ionization rate appears at the same position in space and phase of this heating peak. This can be explained by the fact that the energetic electrons penetrate into the plasma, and still gain energy due to the considerable plasma field, and move further toward the anode until they are repelled by the opposite electric field in the anode sheath. Therefore, the behavior of the energy relaxation in space is somewhat a mixture of nonlocal and local behavior. There is a small energy loss region next to the maximum heating peaking, which corresponds to the electric field reversal region mentioned earlier.

Figures 10(a) and 10(b) show the evolution of the same variables as in Fig. 9 but at a pressure of 400 mTorr. The behavior of the electron heating is quite similar as in the low-pressure case but the ionization profile changes significantly with two peaks at the same position in space and time as the two electron heating peaks. The ionization peak at the anodic presheath and the ionization in the plasma bulk still remain similar to the low-pressure case, but a pronounced ionization peak appears at the cathodic presheath which demonstrates the local behavior of the spatial energy relaxation at high pressure. A similar spatial and temporal ionization profile has been observed at the pressure of 1 Torr in the simulation of SF_6 discharge.[11]

The distinct difference with the argon discharge is, hence, that at both pressure values investigated here, there is always one peak at the momentary anode presheath in the electron heating profile as well as in the ionization profile, and the electron heating and ionization are also considerable in the plasma bulk region.

2. Power effect

The effect of power on the ionization rate for silane discharge has been studied with a fixed frequency at 13.56 MHz and a fixed pressure at 30 mTorr. The spatiotemporal electron heating and ionization are shown in Figs. 11(a) and 11(b) for a power of 25 W compared to the one of 8 W in Fig. 9. The behavior of the electron heating and the ionization is similar as in the lower power case (Fig. 9) except that the value is much higher. Hence, in analogy to the argon discharges, the power does not influence the spatial energy relaxation very much.

3. Frequency effect

The effect of frequency on the ionization rate has been studied with a fixed pressure of 30 mTorr and a fixed power of 8 W. The spatial and temporal behaviors of the electron heating and the ionization rate are shown in Figs. 12(a) and 12(b), respectively for a frequency of 65 instead of 13.56 MHz in Fig. 9. The results look quite different from the lower frequency case: (i) The sheath becomes thinner, in part due to a lower applied voltage. (ii) The electron heating in the plasma bulk and the peak at the anodic presheath, which were strongly present in the low frequency case, become less remarkable at the high frequency. The reason for this is that the plasma field and the relative field maximum at the momentary anodic presheath are much lower and the plasma field is strongly out of phase with the sheath field as shown in Fig. 13. (iii) The field reversal region disappears. At high frequency the negative ion density is found to decrease dramatically compared to the low frequency case, and instead, the electron density increases to compensate the change in the negative charge density. That implies that the electronegative discharge becomes relatively more electropositive at high frequency so that the characteristics of the electronega-

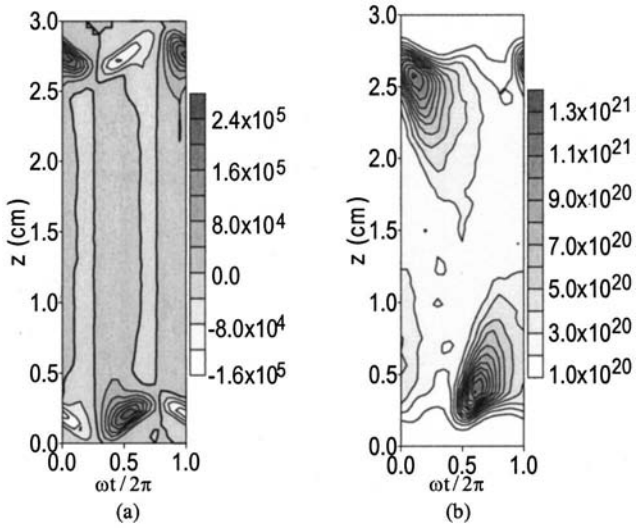

FIG. 12. The variations of (a) electron heating ($W\,m^{-3}$) and (b) ionization rate ($m^{-3}\,s^{-1}$) in space and time for the silane discharge at a higher frequency of 65 MHz. The other parameters are the same as in Fig. 8.

tive discharge will be less pronounced. (iv) The ionization shows some delay compared to the heating, and only one ionization maximum appears at the momentary cathodic presheath in correspondence to the one electron heating peak in time and space. This illustrates that the mean free path for energy loss of the electrons becomes shorter and, hence, the local behavior of the energy relaxation in space becomes more apparent. The delay is due to the fact that at the high frequency the electrons cannot follow the time-varying field very well. The different penetration lengths of the energetic electrons between the high frequency case [in Fig. 12(b)] and the low frequency one [in Fig. 9(b)] result from the different phase relationships between the plasma bulk field and the sheath field [see Figs. 13 and 8(a)]. Indeed, at the high frequency the plasma bulk field is distinctly out of phase with the sheath field, while in the low frequency case it was more or less in phase. In addition to the delay of the ionization

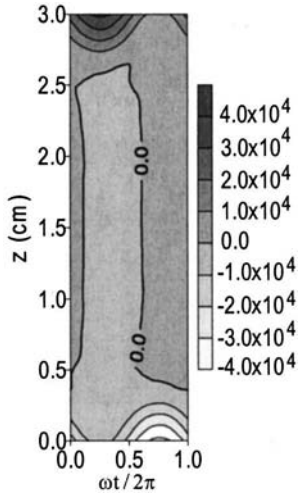

FIG. 13. The variation of the electric field (V/m) in space and time at a higher frequency for the silane discharge. The discharge settings are the same as in Fig. 12.

relative to the heating, at the high frequency the energetic electrons meet the electric field which is opposite to the sheath field earlier in space, i.e., the energetic electrons cannot penetrate into the plasma bulk very deeply.

The difference in the behavior of the ionization rate versus frequency between the argon and the silane discharge is that the silane discharge has fast energy relaxation in space, because the field reversal point in the silane discharge (Fig. 13) is much closer to the momentary cathode than in the argon discharge (Fig. 7).

IV. SUMMARY

The time and space dependence of the electron energy relaxation has been studied and compared through the investigation of the ionization rate between electropositive discharges (argon) and electronegative discharges (silane). The discharge parameters with a pressure of 30 mTorr, a power of 8 W, and a frequency of 13.56 MHz are taken as reference values. A 1D PIC/MC model has been used to describe the rather different behavior of the energy relaxation and the electron heating for the argon and silane discharges with the pressure at 30 and 400 mTorr, the power at 8 and 25 W and the frequency at 13.56 and 65 MHz.

For the argon discharge, there is only one electron heating peak located at the momentary cathodic presheath halfway through the rf cycle. Corresponding to that, at low pressure and low frequency the ionization takes place mainly in the plasma bulk, which is a typical nonlocal effect of the energy relaxation in space. The power does not change the behavior of the electron energy relaxation; it only affects the absolute values of the electron heating and the ionization. With increasing pressure, the energy relaxation shows a local behavior. With increasing frequency the electron energy relaxation tends to exhibit more local behavior since the energetic electrons' penetration becomes shorter. This is attributed to the fact that at high frequency the plasma bulk field is strongly out of phase with the sheath field, i.e., the field reversal curve in the plasma bulk is closer to the cathode, which limits the penetration of the electron in the plasma bulk.

For the silane discharge, at low frequency the behavior of the electron heating and the ionization rate versus pressure and power shows that the electron energy relaxation is similar as in the argon discharge except the following two points. (i) There is always one more ionization peak in correspondence to an additional electron heating maximum located at the momentary anodic presheath. (ii) The electron heating and the ionization in the plasma bulk are considerable due to the nonzero plasma field. Similar to the argon discharge, the power does not change the behavior of the energy relaxation. At high frequency, the electron heating, which is remarkable at the anodic presheath and in the plasma bulk at low frequency, has almost disappeared. Only one ionization peak occurs at the momentary cathodic presheath. This means that the energy relaxation behavior for the silane discharge is similar to the argon discharge, i.e., it tends to a local behavior. The ionization peak is much closer to the cathode than

that in the argon discharge. The energy relaxation in space becomes fast at high frequency.

ACKNOWLEDGMENTS

M. Yan is financed by a New Research Initiative of the University of Antwerp. A. Bogaerts is indebted to the Flemish Fund for Scientific Research (FWO) for financial support. The research of W. J. Goedheer is financed by the Foundation for Fundamental Research on Matter (FOM). The PIC/MC code was developed with financial support from the Netherlands Organization for Scientific Research (NWO). The authors also acknowledge financial support from the Federal Services for Scientific, Technical and Cultural Affairs (DWTC/SSTC) of the Prime Minister's Office through IUAP-IV (Conv. P4/10).

[1] B. Chapman, *Glow Discharge Processes* (Wiley, New York, 1980).
[2] M. A. Lieberman and A. J. Lichtenberg, *Principles of Plasma Discharges and Materials Processing* (Wiley, New York, 1994).
[3] M. J. Kushner, J. Appl. Phys. **64**, 2532 (1988).
[4] Ph. Belenguer and J. P. Boeuf, Phys. Rev. A **41**, 4447 (1990).
[5] S. K. Park and D. J. Economou, J. Appl. Phys. **68**, 3904 (1990).
[6] M. Meyyappan and T. R. Govindan, IEEE Trans. Plasma Sci. **19**, 122 (1991).
[7] M. Surendra, Plasma Sources Sci. Technol. **4**, 56 (1995).
[8] M. J. Colgan, M. Meyyappan, and D. E. Murnick, Plasma Sources Sci. Technol. **3**, 181 (1994).
[9] D. Graves and K. F. Jensen, IEEE Trans. Plasma Sci. **PS–14**, 78 (1986).
[10] J. P. Boeuf, Phys. Rev. A **36**, 2782 (1987).
[11] E. Gogolides and H. H. Sawin, J. Appl. Phys. **72**, 3971 (1992).
[12] D. P. Lymberopoulos and D. J. Economou, J. Phys. D: Appl. Phys. **28**, 727 (1995).
[13] I. B. Bernstein and T. Holstein, Phys. Rev. **94**, 1475 (1954).
[14] L. D. Tsendin, Sov. Phys. JETP **39**, 805 (1974).
[15] S. V. Berezhnoi, I. D. Kaganovich, and L. D. Tsendin, Plasma Sources Sci. Technol. **7**, 268 (1998).
[16] M. Yan, A. Bogaerts, W. J. Goedheer and R. Gijbels (unpublished).
[17] C. K. Birdsall, IEEE Trans. Plasma Sci. **19**, 65 (1991).
[18] V. Vahedi and M. Surendra, Comput. Phys. Commun. **87**, 179 (1995).
[19] T. E. Nitschke and D. B. Graves, J. Appl. Phys. **76**, 5646 (1994).
[20] M. Yan and W. J. Goedheer, IEEE Trans. Plasma Sci. **27**, 1399 (1999).
[21] E. Hamers, Ph.D. thesis, Utrecht University, The Netherlands, 1998.
[22] M. Surendra, D. B. Graves, and G. M. Jellum, Phys. Rev. A **41**, 1112 (1990).
[23] A. K. Jain *et al.*, J. Phys. B **20**, L389 (1987).
[24] M. Kurachi and Y. Nakamura, J. Phys. D **22**, 107 (1989).
[25] E. Krishnakumar and S. K. Srivastava, Contrib. Plasma Phys. **35**, 395 (1995).
[26] P. Haaland, J. Chem. Phys. **93**, 4066 (1990).
[27] J. Perrin *et al.*, Chem. Phys. **73**, 383 (1982).
[28] J. M. S. Henis *et al.*, J. Chem. Phys. **57**, 389 (1972).
[29] A. P. Hickman, J. Chem. Phys. **70**, 4872 (1979).
[30] J. Perrin *et al.*, Contrib. Plasma Phys. **36**, 3 (1996).
[31] M. Surendra and D. B. Graves, Appl. Phys. Lett. **56**, 1022 (1990).
[32] D. Vender and R. W. Boswell, IEEE Trans. Plasma Sci. **18**, 725 (1990).
[33] A. H. Sato and M. A. Lieberman, J. Appl. Phys. **68**, 6117 (1990).
[34] T. J. Sommerer, W. N. G. Hitchon, R. E. P. Harvey, and J. E. Lawler, Phys. Rev. A **43**, 4452 (1991).
[35] R. A. Gottscho and C. E. Gaebe, IEEE Trans. Plasma Sci. **PS–14**, 92 (1986).
[36] R. A. Gottscho and R. H. Mandlich, J. Vac. Sci. Technol. A **3**, 617 (1985).